Visualization for Understanding Uncertainty in the Simulation of Myocardial Ischemia

Paul Rosen, Brett Burton, Kristin Potter, and Chris R. Johnson

Scientific Computing and Imaging Institute
University of Utah

Abstract

We have created the Myocardial Uncertainty Viewer (muView or μView) tool for exploring data stemming from the forward simulation of cardiac ischemia. The simulation uses a collection of conductivity values to understand how ischemic regions effect the undamaged anisotropic heart tissue. The data resulting from the simulation is multi-valued and volumetric and thus, for every data point, we have a collection of samples describing cardiac electrical properties. μView combines a suite of visual analysis methods to explore the area surrounding the ischemic zone and identify how perturbations of variables changes the propagation of their effects.

Categories and Subject Descriptors (according to ACM CCS): J.3 [Computer Applications]: Life and Medical Sciences—Health

1. Introduction

Myocardial ischemia is a disease that results from a metabolic imbalance in which the demand for oxygen and nutrients within the muscular tissue of the heart exceeds local supply, caused by a restriction in blood supply, or ischemia. Left untreated, cardiac cells will gradually weaken and die; in many cases, leading to heart attack. These consequences make ischemic heart disease the leading cause of death for men and women in the U.S. and most industrialized countries [MFB04]. Detection of cardiac ischemia often requires inspecting the results of an electrocardiogram (ECG) and looking for abnormalities, particularly within a specific location within an ECG trace, known as the ST segment. However, we do not fully understand the relationship between cardiac ischemia and abnormalities in the ST segment [TEF*64, FZHD11].

To better understand the underlying physiology of cardiac ischemia, mathematical models are created to study the effect of ischemic regions on cardiac electrical properties, such as the electrical potential outside of a cell, known as extracellular potentials. Striations in cardiac muscle produce an anisotropic conduction pathway along which electrical currents flow that influences resulting tissue potentials. Anisotropy can be captured through diffusion weighted tensor imaging (DTI) using MRI and can be used in forward simulations of cardiac ischemia. Unfortunately, the anisotropy data is usually quite noisy. Defining appropriate tissue conductivities is difficult and has a large impact on the resulting electrical potentials within a simulation of the diseased heart.

We are currently developing the Myocardial Uncertainty Viewer (muView or μView) tool for visualizing the results of cardiac ischemia simulations aimed at understanding the uncertainty present in the forward cardiac problem with respect to tissue conductivities. The goal of μView is to both directly explore the simulation results, helping the scientists design and troubleshoot experiments, and to help understand the relationship of conductivity uncertainties with size and shape estimates of the ischemic zone. The challenges to this goal stem mainly from the complexity of the data; we are given a volumetric model of the heart with multiple simulation outputs for each voxel. The structure of the data is inherently difficult; the spatial domain of the data is 3D, so simply displaying the data causes problems with occlusion and clutter. Indicating further attributes within the 3D context is a formidable challenge. To address this issue, we have created μView to experiment with the use of a collection of visualization techniques, including traditional two-dimensional and three-dimensional displays, as well as the incorporation of information visualization approaches. The broader goal of this work is to develop visualization techniques that can concisely express the nature of the uncertainty within this type of complex data for domain scientists and health care professionals. The bidomain model is a widely accepted computational representation of the electrical response of the heart to

stimuli given defined tissue conductivity and the underlying extracellular and intracellular potentials [Hen93].

2. Background

2.1. A Model of Cardiac Ischemia

Electrocardiographic forward models describe body and cardiac electrical activity (such as surface potentials) that result from electrical sources that lie on or within heart tissue. The bidomain model is a widely accepted computational representation of the electrical response of the heart to stimuli given defined tissue conductivity and the underlying extracellular and intracellular potentials [Hen93]. In this study, the bidomain model was adapted to generate cardiac potentials at a single time instant, under the influence of ischemia. The cardiac source is interpreted as a region of complex geometry, defined by experimental observation, during a single time step within the cardiac cycle (a heartbeat). Tissue within the diseased region was assigned reduced conductivity and transmural potential values.

Given the variability in reported cardiac tissue conductivities [Joh03, JK03, Cle76, RHS79, RS82], we simulate over a selected range of values to represent longitudinal and transmural conductivities within the intracellular and extracellular cardiac spaces. We applied second order *generalized polynomial chaos-stochastic collocation* (gPC-SC) [Xiu07] to the conductivity ranges, shown in Table 1, to select pertinent conductivities within the range and reduce complexity of the overall model. This method produced a series of 41 distinct conductivity combinations to use as input to the multi-run forward simulation based on the passive bidomain equations.

Table 1: *Conductivity Ranges*

	Longitudinal		Transmural	
	σ_i	σ_e	σ_i	σ_e
Min	0.00174	0.0012	0.000193	0.0008
Max	0.0034	0.00625	0.0006	0.00236
Isch. Scaling	1/10	1/2	1/1000	1/4

Ultimately, the outputs produced are 41 simulations, each of which has a single scalar voltage associated with each data point. The data points will therefore each have 41 independent scalar values associated with them. In addition to the output data, we can leverage input data, such as the tetrahedral or hexahedral mesh data or DTI data.

2.2. Uncertainty Visualization

Interest in uncertainty visualization has increased during the past few years [GS06, JS03, MRH*05, PWL97], and the topic has been identified as a top research problem [Joh04]. Related to this work are techniques aimed at incorporating uncertainty information into volume rendering and isosurfaces, using linked multiple windows, the visual representation of probability distribution functions (PDFs), and displaying the results of parameter-space explorations.

Volume rendering and isosurfacing are techniques designed to convey spatial characteristics of volumetric scalar data. Approaches to add uncertainty information include pseudo-coloring, overlay, transparency, glyphs and animation [DKLP02, JLRP99, LLPY07, RLBS03]. Fout and Ma [FM12] propose a computational model that computes a posteriori bounds on uncertainty propagated through the entire volume rendering algorithm and developed an interactive tool to inspect the resulting uncertainty.

Rather than using isosurfaces to directly convey uncertainty in data, they can be used to show shape and extent of clusters [Luc06]. Probabilistic formulations of marching cubes [PWH11] and isocontours [PH10] allow for the display of positional uncertainty of isosurfaces colored by their distance from a mean [PRW11].

While these three-dimensional representations are quite useful for conveying geometric structure and providing context, the complexity of the data often requires multiple presentation types to enable full understanding. For this reason multi-window linked-view systems are popular for addressing uncertainty [FKLI10a, HMH08, PWB*09, SZD*10].

Another way to look at uncertainty is to consider the multiple values as PDFs and to use statistical methods for characterizing them. Initial work in the area began by extending existing techniques to work with PDFs [LKP03]. Clustering [BKS04] and slice planes [KLDP02] can be used to reduce the dimensionality of the data for visualization, while colormaps, glyphs, and deformations have been used to express summaries and clusters [KDP01, KKL*05].

Finally, the type of data we are looking at here can be thought of in terms of parameter-space exploration in which the effect of perturbations of input parameters is related visually to outcomes through techniques such as parallel coordinates [BPFG11] and preattentive highlighting [FKLI10b].

3. Visualization System

μView is an interactive 5-way linked view system, where the main view contains a 3D visualization of the data (Figure 1 A), three side views contain orthogonal 2D slices through the volume (Figure 1 B-D), and finally, a parallel coordinates view of the PDFs (Figure 1 E). All interfaces are manipulated through mouse interactions and a small menu system.
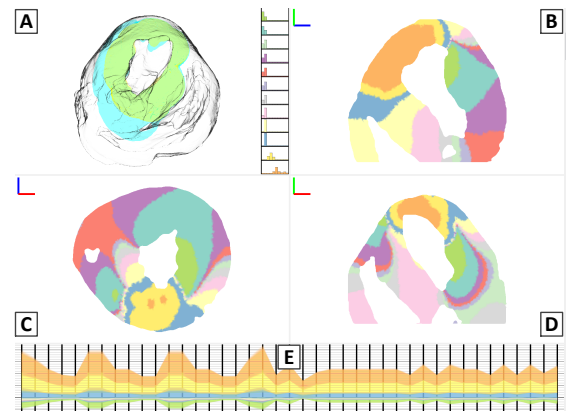

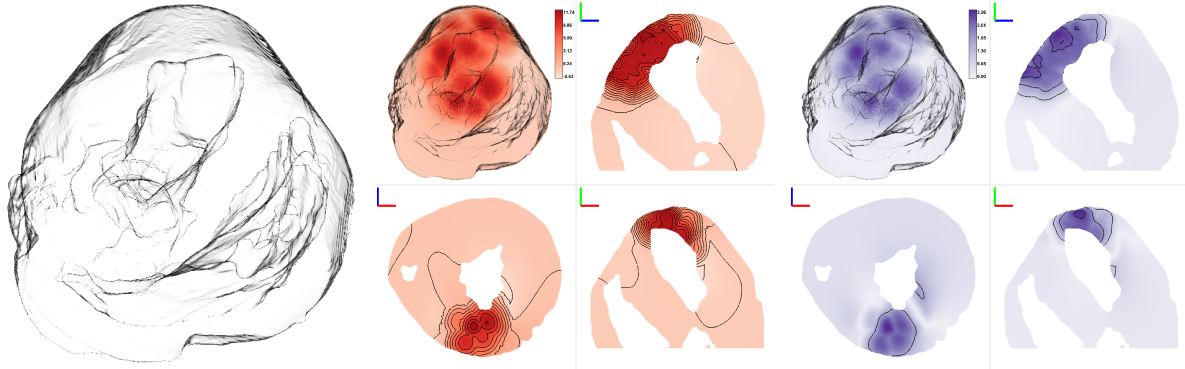**Figure 1:** *Overview of user interface. A: 3D view, B-D: 2D views, E: parallel coordinates.*

Figure 2: *Silhouettes are calculated for the surface model and used for context (left). Single value color sequential mapping of mean value (middle) and standard deviation (right).*

The data input into our system consists of three components. The first is a set of vertices. Second, a solid mesh of tetrahedral or hexahedral elements connects the vertices and forms the anatomy of the heart. Finally, an ensemble of simulation results are attached to each vertex in the mesh.

3.1. Visual Interfaces

3D View: Anatomic context is important in medical applications and thus we provide a 3D rendering of the geometry. Using a surface mesh extracted from the volume, we darken triangle faces that are near perpendicular to the view direction to help in understanding 3D shape, as seen in Figure 2, left. Within this interface, the data can then be visualized either through a series of isosurfaces as discussed in Section 3.2 or by rendering the data points colored via a transfer function as discussed in Section 3.3.

2D View: For 2D visualization, slices of the volume are extracted by intersecting the solid elements with a plane and linearly interpolating vertices, triangles, and PDFs. The three slice planes, axial, coronal, and sagittal, are a more natural way for health care professionals to view the data, and are displayed using transfer functions to color the mesh and isolines to help highlight the ischemic zone. Orientation planes (not shown) can be added to the 3D visualization to help users identify the 3D spatial location of the slices.

Parallel Coordinate View: Parallel coordinate are an alternative way to explore the high-dimensional space of the data. We supply a parallel coordinates interface where each dimension represents a single ensemble dimension, providing an overview of the whole data set. The lines within the display are colored using the same transfer function as in the other linked-views. This enables the user to directly correlate the values seen in the 3D visualization to those of the values present in the data. For example, in Figure 1 it can be seen in the parallel coordinates that the orange colored cluster is likely enclosing the ischemic zone. Similar observations are true of the other clusters as well, though some are difficult to see because of their limited value range in the parallel coordinate view.

3.2. Isosurfaces over the PDFs

The range of values for an individual data point makes isosurface location unclear [JPGJ12]. Each dimension may maintain its own isosurface for a given isovalue, meaning the isosurface for the PDF could exist anywhere within a range of locations. To account for this, we reduce the PDF to a single dimension by applying an operator, such as minimum, maximum, or mean, to the data samples at each point. Isosurfaces are then extracted from the single dimensional field. Figure 4 shows an example where the minimum isosurface is blue and the maximum isosurface is yellow implying an envelope containing the range of possible surfaces.

3.3. Transfer Functions over the PDFs

Because of the complexity of the data, we have adopted a number of transfer functions to color the data, each designed to aid understanding in a unique way.

Value-based Coloring: The first transfer function simply assigns a single value to each data point and applies an intensity-based sequential color map. The values can be related to individual dimensions, or derived values such as the mean (Figure 2 middle) or standard deviation (Figure 2 right).

Coloring by Clustering: Clustering can reduce the set of data under investigation by grouping similar data together, such as points that respond similarly to variations in initial conditions. We use K-means clustering [M*67] to exploring this space and employ multiple distance metrics. The L2-norm (Figure 3 left) groups points that are similar in a Euclidean sense and is defined by $d(X,Y) = \sqrt{\sum (X_i - Y_i)^2}$, where X and Y each contain the 41 simulation dimensions of data points.

Pearson correlation coefficient [RN88] (Figure 3 right) clusters points that respond similarly to changes in input and is defined as $d(X,Y) = 1 - \frac{\sum (X_i - \overline{X})(Y_i - \overline{Y})}{\sqrt{\sum (X_i - \overline{X})}\sqrt{\sum (Y_i - \overline{Y})}}$, where $\overline{X}$ and $\overline{Y}$ are the means of the sets.

As points are placed into clusters, they are colored using a categorical color map. A collection of histograms showing the mean of each cluster is shown to the right.

Coloring by Isovalue: As a final alternative, we have explored coloring points by isovalue. This method takes each PDF and counts the number of dimensions above and below

the isovalue. In this scheme, we choose solid colors to represent data points where all dimensions were above (red) or below (blue) the isovalue. The remaining points are colored using a sequential color map (orange to blue-green) which partially indicate how many dimensions fall above or below the isovalue. An example is seen in Figure 4, right.

4. Preliminary Results

Our initial experiments have been performed primarily on a mesh created by MRI segmentations of an excised canine heart with atrial tissue removed. The mesh consists of 1.4M tetrahedra, 350K vertices, and 41 simulations. Our software takes a few moments to load data (15-30 seconds) and a few seconds to apply some operators (1-60 seconds; clustering being the slowest), but overall the software is interactive.

We developed this tool as part of a team of visualization and biomedical researchers to better understand the physiology of cardiac ischemia. μView is being actively developed simultaneously with the development of the simulation model, allowing results from the simulation to be explored within μView, and the insights gleaned from μView to be incorporated back into the simulation. While our results to date are still in the experimental phase, we have already had some success within this collaboration.

The conductivities of the heart are highly dependent on the fiber directions across the tissue. The fiber direction data can be created any number of ways, such as rule-based methods or, as in our case, using DTI. Part of our study is understanding the sensitivity of conductivity to fiber direction.

As we began our study, we noticed a bulge for many isovalues (most prominently visible as the yellow area in Figure 4 right) that we could not easily explain. We then dove into the data by directly visualizing some of the input, such as fiber direction. This lead us to discover that the fiber directions from our DTI imaging were noisy and poorly aligned for the first few millimeters of the heart surface. While we have not yet confirmed that the erroneous fiber directions have a significant influence on the bulge, this finding did steer us to redesign our input by obtaining a more accurate model, either through better imaging or a rule-based method.

5. Future Work

This work is an initial exploration of uncertainty data obtained from the forward simulation of cardiac ischemia, and
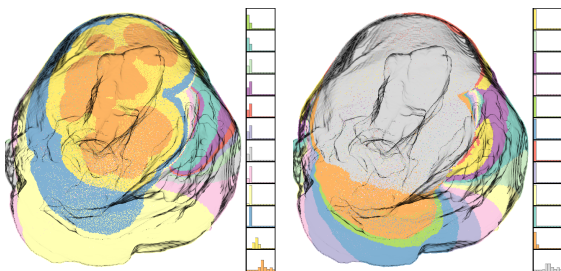

Figure 3: *K-means clustering applied to the data using the L2-Norm (left) and Pearson correlation coefficient (right) as distance metrics.*
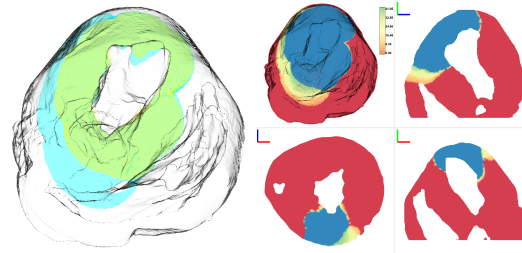

Figure 4: *Left: Isovalue visualization using isosurfacing to describe the range of potential isosurfaces of a given value. Right: Isovalue color mapped by counting dimensions above and below the isovalue.*

thus we still have much work yet to do. We believe our close collaboration with the simulation scientists will greatly guide the choices we make regarding visualization, particularly in light of our discovery of irregular fiber directions. Such a discovery also encourages the question of the importance of fiber direction, which we plan to further investigate through techniques such as those proposed by Jones [Jon03] for visualizing uncertainty in fiber orientation.

The ultimate clinical goal is to be able to assess the uncertainty in determining the ischemic zone from an inverse simulation linked to ST segment waveform changes. If we better understand how the uncertainty in the conductivities affect the size and shape of the ischemic zone, it will help determine what levels of uncertainty will be of consequence clinically and how much confidence to assign to the understanding of the ischemic zone size, shape, and location.

Additionally, from a scientific point of view, these studies can also give us a better understanding of the relationship of conductivity uncertainty to both forward and inverse simulations of cardiac ischemia. In the future, we aim to provide confidence criteria of the simulation results as a function of both conductivity uncertainty and the problem we are trying to solve. It may be that for some problems, the level of uncertainty will not greatly effect the results, while for other applications, the uncertainty will invalidate an approach. It may also indicate that uncertainty levels in the conductivities would have to be reduced in order to use such a method for a particular application, which could then spark research into generating better conductivity values.

Both clinical problems and scientific exploration provide opportunities for improvement in uncertainty visualization techniques, and we look forward to extending μView to have greater research and clinical impact.

References

[BKS04] BORDOLOI U. D., KAO D. L., SHEN H.-W.: Visualization techniques for spatial probability density function data. *Data Science Journal 3* (2004), 153–162. 2

[BPFG11] BERGER W., PIRINGER H., FILZMOSER P., GRÖLLER E.: Uncertainty-aware exploration of continuous parameter spaces using multivariate prediction. *Comp. Graph. Forum 30*, 3 (2011), 911 – 920. 2

[Cle76] CLERC L.: Directional differences of impulse spread in trabecular muscle from mammalian heart. *J. Physiol. 255* (1976), 335–346. 2

[DKLP02] DJURCILOV S., KIM K., LERMUSIAUX P., PANG A.: Visualizing scalar volumetric data with uncertainty. *Computers and Graphics 26* (2002), 239–248. 2

[FKLI10a] FENG D., KWOCK L., LEE Y., II R. M. T.: Linked exploratory visualizations for uncertain mr spectroscopy data. *SPIE Vis. and Data Analysis 7530*, 4 (2010), 1–12. 2

[FKLI10b] FENG D., KWOCK L., LEE Y., II R. M. T.: Matching visual saliency to confidence in plots of uncertain data. *IEEE TVCG 16*, 6 (2010), 980–989. 2

[FM12] FOUT N., MA K.-L.: Fuzzy volume rendering. *IEEE TVCG 18*, 12 (2012), 2335–2344. 2

[FZHD11] FLEISCHMANN K. E., ZÏ£¡GRE-HEMSEY J., DREW B. J.: The new universal definition of myocardial infarction criteria improves electrocardiographic diagnosis of acute coronary syndrome. *J Electrocardiol. 44* (2011), 69–73. 1

[GS06] GRIETHE H., SCHUMANN H.: Visualization of uncertain data: Methods and problems. In *SimVis* (2006), pp. 143–156. 2

[Hen93] HENRIQUEZ C.: Simulating the electrical behaviour of cardiac tissue using the bidomain model. *Crit. Rev. Biomed. Eng 21*, 1 (1993), 1–77. 2

[HMH08] HAROZ S., MA K.-L., HEITMANN K.: Multiple uncertainties in time-variant cosmological particle data. In *IEEE PacificVis* (2008), pp. 207–214. 2

[JK03] JOHNSTON P. R., KILPATRICK D.: The effect of conductivity values on st segment shift in subendocardial ischaemia. *IEEE Trans. Biomedical Eng. 50* (2003), 150–158. 2

[JLRP99] JOSPEH A. J., LODHA S. K., RENTERIA J. C., PANG A.: Uisurf: Visualizing uncertainty in isosurfaces. In *Computer Graphics and Imaging* (1999), pp. 184–191. 2

[Joh03] JOHNSTON P. R.: A cylindrical model for studying subendocardial ischaemia in the left ventricle. *Mathematical Biosciences 186* (2003), 43–61. 2

[Joh04] JOHNSON C. R.: Top scientific visualization research problems. *IEEE CG&A 24*, 4 (2004), 13–17. 2

[Jon03] JONES D. K.: Determining and visualizing uncertainty in estimates of fiber orientation from diffusion tensor mri. *Magnetic Resonance in Medicine 49* (2003), 7–12. 4

[JPGJ12] JIAO F., PHILLIPS J., GUR Y., JOHNSON C.: Uncertainty visualization in HARDI based on ensembles of ODFs. In *IEEE PacificVis* (2012), pp. 193–200. 3

[JS03] JOHNSON C., SANDERSON A.: Next step: Visualizing errors and uncertainty. *IEEE CG&A 23*, 5 (2003), 6–10. 2

[KDP01] KAO D., DUNGAN J. L., PANG A.: Visualizing 2d probability distributions from eos satellite image-derived data sets: a case study. In *IEEE Vis* (2001), pp. 457–561. 2

[KKL*05] KAO D., KRAMER M., LUO A., DUNGAN J., PANG A.: Visualizing distributions from multi-return lidar data to understand forest structure. *Cartogr. J. 42*, 1 (2005), 35–47. 2

[KLDP02] KAO D., LUO A., DUNGAN J. L., PANG A.: Visualizing spatially varying distribution data. In *Information Visualisation* (2002), pp. 219–225. 2

[LKP03] LUO A., KAO D., PANG A.: Visualizing spatial distribution data sets. In *Symp. on Data Vis.* (2003), pp. 29–38. 2

[LLPY07] LUNDSTRÖM C., LJUNG P., PERSSON A., YNNERMAN A.: Uncertainty visualization in medical volume rendering using probabilistic animation. *IEEE TVCG 13*, 6 (2007), 1648–1655. 2

[Luc06] LUCIEER A.: Visualization for exploration of uncertainty related to fuzzy classification. In *IEEE Itnl Conf on Geoscience and Remote Sensing* (2006), pp. 903–906. 2

[M*67] MACQUEEN J., ET AL.: Some methods for classification and analysis of multivariate observations. In *Berkeley Symp. on Math. Stat. and Prob.* (1967), vol. 1, p. 14. 3

[MFB04] MATHERS C. D., FAT D. M., BOERMA J. T.: *The Global Burden of Disease: 2004 Update*. Tech. rep., World Health Organization, 2004. 1

[MRH*05] MACEACHREN A. M., ROBINSON A., HOPPER S., GARDNER S., MURRAY R., GAHEGAN M., HETZLER E.: Visualizing geospatial information uncertainty: What we know and what we need to know. *Cartography and Geographic Information Science 32*, 3 (2005), 139–160. 2

[PH10] PÖTHKOW K., HEG H.-C.: Positional uncertainty of isocontours: Condition analysis and probabilistic measures. *IEEE TVCG PP*, 99 (2010), 1–15. 2

[PRW11] PFAFFELMOSER T., REITINGER M., WESTERMANN R.: Visualizing the positional and geometrical variability of isosurfaces in uncertain scalar fields. *Comp. Graph. Forum 30*, 3 (2011), 951–960. 2

[PWB*09] POTTER K., WILSON A., BREMER P.-T., WILLIAMS D., DOUTRIAUX C., PASCUCCI V., JOHHSON C. R.: Ensemble-vis: A framework for the statistical visualization of ensemble data. In *IEEE Workshop on Knowledge Discovery from Climate Data: Prediction, Extremes.* (2009), pp. 233–240. 2

[PWH11] PÖTHKOW K., WEBER B., HEGE H.-C.: Probabilistic marching cubes. *Comp. Graph. Forum 30*, 3 (2011), 931–940. 2

[PWL97] PANG A., WITTENBRINK C., LODHA. S.: Approaches to uncertainty visualization. *Vis. Comp. 13*, 8 (1997), 370–390. 2

[RHS79] ROBERTS D. E., HERSH L. T., SCHER A. M.: Influence of cardiac fiber orientation on wavefront voltage, conduction velocity and tissue resistivity in the dog. *Circ. Res 44* (1979), 701–712. 2

[RLBS03] RHODES P. J., LARAMEE R. S., BERGERON R. D., SPARR T. M.: Uncertainty visualization methods in isosurface rendering. In *Eurographics Short Papers* (2003), pp. 83–88. 2

[RN88] RODGERS J. L., NICEWANDER W. A.: Thirteen ways to look at the correlation coefficient. *The American Statistician 42*, 1 (1988), 59–66. 3

[RS82] ROBERTS D. E., SCHER A. M.: Effects of tissue anisotropy on extracellular potential fields in canine myocardium in situ. *Circ. Res 50* (1982), 342–351. 2

[SZD*10] SANYAL J., ZHANG S., DYER J., MERCER A., AMBURN P., MOORHEAD R. J.: Noodles: A tool for visualization of numerical weather model ensemble uncertainty. *IEEE TVCG 16*, 6 (2010), 1421 – 1430. 2

[TEF*64] TOYOSHIMA H., EKMEKCI A., FLAMM E., MIZUNO Y., NAGAYA T., NAKAYAMA R., YAMADA K., PRINZMETAL M.: Angina pectoris vii. the nature of st depression in acute myocardial ischaemia. *Am. J. Cardiology 13* (1964), 498–509. 1

[Xiu07] XIU D.: Efficient collocational approach for parametric uncertainty analysis. *Comm. Comp. Phys. 2* (2007), 293–309. 2